technical note technical note

Predicting the Burning Rates of Noncharring Polymers

July 2009

DOT/FAA/AR-TN09/16

U.S. Department of Transportation
Federal Aviation Administration

NOTICE

This report is available at the Federal Aviation Administration William J. Hughes Technical Center's Full-Text Technical Reports page: actlibrary.act.faa.gov in Adobe Acrobat portable document format (PDF).

Technical Report Documentation Page

1. Report No.	2. Government Accession No.	3. Recipient's Catalog No.
DOT/FAA/AR-TN09/16		

4. Title and Subtitle	5. Report Date
PREDICTING THE BURNING RATES OF NONCHARRING POLYMERS	July 2009
	6. Performing Organization Code

7. Author(s)	8. Performing Organization Report No.
Stanislav I. Stoliarov*, Sean Crowley, and Richard E. Lyon	

9. Performing Organization Name and Address	10. Work Unit No. (TRAIS)
*SRA International, Inc. 1201 New Road, Suite 242 Linwood, NJ 08221	
Federal Aviation Administration William J. Hughes Technical Center NextGen & Operations Planning Airport and Aircraft Safety Research and Development Division Fire Safety Branch Atlantic City International Airport, NJ 08405	11. Contract or Grant No.

12. Sponsoring Agency Name and Address	13. Type of Report and Period Covered
U.S. Department of Transportation Federal Aviation Administration Air Traffic Organization NextGen & Operations Planning Office of Research and Technology Development Washington, DC 20591	Technical Note
	14. Sponsoring Agency Code ANM-115

15. Supplementary Notes

16. Abstract

This study provides a thorough examination of whether a numerical pyrolysis model, which describes transient energy transport and chemical reactions taking place in a one-dimensional object, can be used as a practical tool for prediction and/or extrapolation of the results of fire calorimetry tests. The focus is on noncharring polymers, in particular—poly(methylmethacrylate), high-impact polystyrene, and high-density polyethylene. First, relevant properties of these materials were measured and/or obtained from the literature. Subsequently, the values of these properties were used to simulate gasification and cone calorimetry experiments, which were performed under a broad range of conditions. A comparison with the experimental results indicates that the model gives reasonably good predictions of the mass loss and heat release histories. It also predicts the evolution of temperature inside the material samples.

17. Key Words	18. Distribution Statement
Material flammability, Gasification, Cone calorimetry, Pyrolysis model, ThermaKin	This document is available to the U.S. public through the National Technical Information Service (NTIS), Springfield, Virginia 22161.

19. Security Classif. (of this report)	20. Security Classif. (of this page)	21. No. of Pages	22. Price
Unclassified	Unclassified	41	

ACKNOWLEDGEMENTS

Certain commercial equipment, instruments, and materials are identified in this technical note to adequately specify the procedure. Such identification does not imply recommendation or endorsement by the Federal Aviation Administration. The authors are very grateful to Dr. Gregory Linteris and Dr. Takashi Kashiwagi of the National Institute of Standards and Technology for help with the gasification experiments and thermal conductivity measurements. The authors also would like to thank Richard Walters of the Federal Aviation Administration and Natallia Safronava of SRA International, Inc. for performing thermogravimetric and microscale combustion calorimetry measurements.

TABLE OF CONTENTS

LIST OF FIGURES

LIST OF TABLES

LIST OF ACRONYMS AND SYMBOLS

α	Absorption coefficient
ρ	Density
τ	Transmissivity
A	Arrhenius pre-exponential factor
c	Heat capacity
E	Activation energy
h_C	Heat of combustion of volatile decomposition products
h_D	Heat of decomposition reaction
K	Kelvin
k	Thermal conductivity
k_D	Rate constant of decomposition reaction
l	Thickness
m	Mass
r	Reflectivity
R	Gas constant
T	Temperature
t	Time
T_{bottom}	Bottom-surface temperature
T_{top}	Top-layer temperature
T_{trans}	Solid-liquid transition temperature
EHF	External heat flux
HDPE	High-density polyethylene
HIPS	High-impact polystyrene
HRR	Heat release rate
MLR	Mass loss rate
PMMA	Poly(methylmethacrylate)
PS	Polystyrene

EXECUTIVE SUMMARY

The results of this study demonstrate that a one-dimensional numerical pyrolysis model called ThermaKin, which was developed by SRA International, Inc. and the Federal Aviation Administration, can be used to predict the outcome of gasification and cone calorimetry experiments performed on a noncharring polymer. The predictions require the knowledge of chemical (decomposition kinetics and thermodynamics), thermal (density, heat capacity, and thermal conductivity), and optical (reflectivity and absorption coefficient) properties of the material. Most of these properties can be measured in milligram-scale laboratory tests or calculated from molecular structure. This work represents the first step toward development of a comprehensive computational methodology for assessment of the impact of ultra-fire-resistant materials and material substitutions on the likelihood of an in-flight fire and the severity of a post-crash fire.

INTRODUCTION

It has been demonstrated by a number of studies [1-3] that a numerical pyrolysis model can be used effectively to analyze relationships between the fundamental physical and chemical properties of a polymeric material (synthetic or natural) and its gasification behavior. In a typical application, the model, which includes transient heat transfer coupled with simplified decomposition chemistry, is used to compute the mass loss rate (MLR) from a one-dimensional material object exposed to external heat. This study extends the previous work by providing a thorough examination of whether such a model can be employed as a practical tool for prediction and/or extrapolation of the results of fire calorimetry experiments.

The focus is on noncharring polymers, in particular—poly(methylmethacrylate) (PMMA), high-impact polystyrene (HIPS), and high-density polyethylene (HDPE). First, thermal, optical, and chemical properties of these materials were measured and/or obtained from the literature. An effort was made to perform an accurate and comprehensive characterization of each material. Subsequently, these materials were subjected to a series of gasification [4] and cone calorimetry [5] tests. The cone calorimetry experiments (which are used to measure the heat release rate (HRR) by a burning material) were performed under a broad range of conditions. The external heat flux was varied between 23 and 75 kW m^{-2}; the initial sample thickness was varied between 3.0×10^{-3} and 2.9×10^{-2} m. In some experiments, the measurement of HRR was accompanied by the measurement of temperature inside the material sample.

A one-dimensional numerical pyrolysis model called ThermaKin was used to simulate these tests. ThermaKin is a flexible computational framework that solves energy and mass conservation equations, which are formulated in terms of rectangular finite elements. A material is represented by a set of components, which may undergo chemical and physical interactions. The number of components and the number and nature of their interactions is dictated by the availability of the quantitative information on the processes that take place inside the material. In the current study, the descriptions of PMMA, HIPS, and HDPE were formulated on the basis of the information that was obtained from the property measurements. The initial and boundary conditions were set to match the conditions of the gasification and cone calorimetry experiments. A description of the model setup, which includes an outline of the key processes that were modeled, is given in the next section. A detailed description of ThermaKin, including its mathematical formulation and numerical algorithms, can be found in references 6 and 7.

MODELING

Within the ThermaKin framework, each polymer was represented by 3 or 4 components. Physical properties of a polymer below and above the solid-liquid transition temperature (T_{trans}) were described by components S and L, respectively. Components G and C represented the products of polymer decomposition. The components were linked by the following first order reactions:

$$S \rightarrow L \quad (1)$$

$$L \rightarrow S \quad (2)$$

$$L \rightarrow G + C \quad (3)$$

Above T_{trans}, the rate of reaction 1 was defined by 1 s^{-1} rate constant. Below T_{trans}, the rate was set to 0. The opposite was true for reaction 2. This reaction took place (with the rate constant of 1 s^{-1}) when the temperature fell below T_{trans}. In the case of PMMA and HIPS, reaction 1 and 2 were used to simulate an apparent glass transition. The rate constant was chosen in such a way that, on the time scale of the simulations, this transition was essentially instantaneous. In the case of HDPE, these reactions were used to simulate melting and crystallization. The heat of reaction 1 was assigned the heat of melting (reported below). The heat of reaction 2 was assigned the same value of heat with the opposite sign (for PMMA and HIPS, the heats of reaction 1 and 2 were set to 0).

The rate constant of reaction 3 (k_D) was defined by the Arrhenius expression:

$$k_D = A\exp\left(-\frac{E}{RT}\right) \quad (4)$$

where A is the pre-exponential factor; E is the activation energy; R is the gas constant; and T is temperature. The thermodynamics of this reaction was defined by the heat of decomposition, which was the sum of the heat of formation and heat of vaporization of decomposition products. PMMA and HDPE decomposition products were represented by one component, G. HIPS decomposed to 98% (by mass) of G and 2% of C. Component C was used to represent the nonvolatile residue that this polymer produced during the gasification and combustion. Both G and C were assigned the same physical properties as component L. G was the only component that was designated as a gas, which means that it can undergo mass transfer. In ThermaKin, mass transfer is driven by a concentration gradient and defined by the gas transfer coefficient. The value of this coefficient was set sufficiently high (1×10^{-5} m^2 s^{-1} for all components representing a polymer) to ensure that the flux of G out of a material object was always equal to the rate of its production inside the object. In other words, the mass transfer was made so fast that it had no effect on the rate of mass loss. Under these conditions, the concentration of G inside the object was always negligible.

The primary mode of energy transfer inside all materials was conduction. In-depth absorption of the radiative energy flux from the flame and/or external heater was also taken into account by using the random absorption algorithm [6 and 7]. In this algorithm, a random sampling (performed at the frequency of 1 per time step) is used to distribute the energy inside a one-dimensional object in accordance with the assumption of exponential attenuation (Beer-Lambert law). The emission (loss) of radiative energy is also computed using this sampling, which means that, at any given time, the object absorbs and emits radiation at/from the same depth. In the current setup, all components representing a given polymer were assumed to have identical absorption coefficients and emissivities. The emissivities were calculated as 1 minus reflectivity.

The one-dimensional objects that were used to model the gasification and cone calorimetry experiments consisted of two layers. The top layer, which represented a polymer sample, was initially composed of component S. The initial thickness of this layer was taken to be equal to the initial sample thickness. The bottom layer consisted of component U that represented an insulating material used in the experiments. This component was assigned the thermal properties of Foamglas® (used in the gasification tests) or a Kaowool™ blanket (used in the cone calorimetry). Their densities (ρ), heat capacities (c), and thermal conductivities (k), which were obtained from the manufacturers, are listed in table 1. To simulate the presence of aluminum foil between the sample and insulator, the gas transfer coefficient and emissivity of component U were set to 0. The insulating layer was specified to be 0.013 m thick. Doubling the thickness did not produce any significant changes in the results of the simulations. The initial temperature of both layers was always set at 298 Kelvin (K).

Table 1. Properties of Insulating Materials

Material	ρ (kg m^{-3})	c (J kg^{-1} K^{-1})	k (Wm^{-1} K^{-1})
Foamglas	120	840	0.08[b]
Kaowool blanket	48	800[a]	0.08[b]

[a] This value was estimated from the material composition (50% of silica and 50% of alumina).
[b] This value was measured at about 500 K.

The top surface of the objects was specified to have no resistance to the outward gas flow. The surface was exposed to the same radiative external heat flux (EHF) that was measured in the corresponding experiment. In the case of cone calorimetry, the radiative heating that took place before ignition was accompanied by convective cooling. The convection was defined by a convection coefficient of 8.2 Wm^{-2} K^{-1} and an outside temperature of 298 K. The value of the coefficient was obtained by using a formula for the natural convection from a horizontal plate in air [8]. The plate had the dimensions of the cone calorimetry specimen holder (0.115 $\times$ 0.115 m). The temperature of the plate was taken to be 484 K, which is half way between the room temperature (298 K) and the mean of the experimental top-layer temperatures (reported below). The bottom surface of the objects was defined to be completely impenetrable to heat and mass flows.

The energy and mass conservation equations were solved by subdividing the objects into 5×10^{-5} m thick elements and using a 0.01 s time step. Reducing these integration parameters by an order of magnitude did not produce any significant changes in the results of the simulations. MLR histories were obtained by recording the mass flux of component G out of the top surface. In the simulations of the cone calorimetry tests, MLR was converted to HRR by multiplying it by the corresponding mean value of the total heat released (reported below). An ignition of the top surface was specified to occur when HRR exceeds 10 kW m^{-2} (this value of the threshold gave the best agreement between the times to ignition determined from experimental HRR histories and the corresponding times of appearance of a sustained flame recorded by an operator). The

flame was modeled by turning off the convective cooling and adding a constant radiative heat flux onto the surface.

EXPERIMENTAL

PROPERTY MEASUREMENTS.

DENSITY. The polymers used in this study were provided in the form of large (approximately 2 m × 1 m) sheets, which were about 6×10^{-3} m thick. The information on the polymers is summarized in table 2. Room temperature densities were determined by measuring dimensions of 0.1 kg to 0.2 kg rectangular pieces of these materials. The densities of PMMA, HIPS, and HDPE were found to be 1200 kg m^{-3}, 1030 kg m^{-3}, and 960 kg m^{-3}, respectively. Literature density data [9] for PMMA, polystyrene (PS), and HDPE are plotted in figure 1 (points) as a function of temperature. The literature values at room temperature are within 2% of those measured in this work. On the basis of this agreement, it was assumed that the literature data provide a sufficiently accurate description of the variation of density with temperature for the materials under study.

Table 2. Polymers Used in This Study

Polymer	Color	Manufacturer	Trade Name
PMMA	Clear	Atofina Chemicals, Inc.	Plexiglas G®
HIPS	White	Westlake Plastics Company	HIPS
HDPE	White	Poly Hi Solidur, Inc.	HD Natural SR

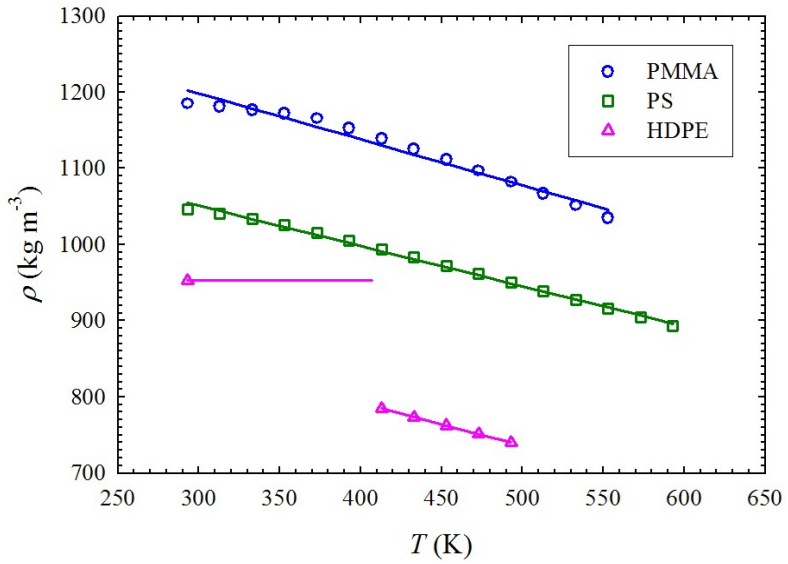

Figure 1. Polymer Densities

The density data were reduced by fitting them with linear functions:

$$\rho = \rho_0 + \rho_1 T \tag{5}$$

In the case of HDPE, it was assumed that below its 407 K melting point the density is constant. The melting point of HDPE was determined in a previous work [10]. The results of the data reduction are shown as lines in figure 1. The parameters of the fitted functions are given in table 3.

Table 3. Parameters (of equation 5) Describing Temperature Dependence of Density

Polymer	Temperature Range	ρ_0 (kg m^{-3})	ρ_1 (kg m^{-3} K^{-1})
PMMA	–	1380	-0.60
HIPS	–	1210	-0.53
HDPE	T<407 K	950	0
	T≥407 K	1010	-0.56

HEAT CAPACITY. The heat capacities of PMMA, HIPS, and HDPE were measured in a previous study [10] using differential scanning calorimetry. The results of those measurements were expressed using a piecewise linear function:

$$c = \begin{cases} c_{S0} + c_{S1} T, & T < T_{trans} \\ c_{L0} + c_{L1} T, & T \geq T_{trans} \end{cases} \tag{6}$$

The parameters of this function, which were converted to be used with temperature in K, are listed in table 4. Among the three polymers, melting was detected only for HDPE. The heat of melting (which took place at T_{trans} = 407 K) was determined to be 2.2×10^5 J kg^{-1}.

Table 4. Parameters (of equation 6) Describing Temperature Dependence of Heat Capacity

Polymer	c_{S0} (J kg^{-1} K^{-1})	c_{S1} (J kg^{-1} K^{-2})	T_{trans} (K)	c_{L0} (J kg^{-1} K^{-1})	c_{L1} (J kg^{-1} K^{-2})
PMMA	-1330	8.6	403	1120	2.4
HIPS	-660	6.4	421	1710	0.7
HDPE	-1040	9.0	407	370	5.1

THERMAL CONDUCTIVITY. Thermal conductivity was measured using a Thermoflixer™ apparatus (SWO Polymertechnik GmbH), which is based on the transient line source method [11]. A bubble-free sample of polymer melt was obtained by repeatedly inserting and compressing small amounts of polymer into a cylindrical sample container (0.010 m in diameter and 0.025 m in length). The container was located in the center of a temperature-controlled oven. A thin probe containing a heater wire and thermocouple was inserted along the axis of the

container into the molten sample. Thermal conductivity was determined from a small (2 to 5 K) change in the probe temperature that occurred within the first 10 s of power output from the probe heater. The measurements were performed in the temperature range between 315 K and the stability limit, which was set to be 50 K below the temperature at which the polymer begins to loose mass (the mass loss information was obtained from the thermogravimetric analyses described below).

The results of the measurements are shown as points in figure 2. For PMMA, the thermal conductivity is significantly lower than the values reported in the literature [12], 0.19 W m^{-1} K^{-1} at 273 to 323 K and 0.25 W m^{-1} K^{-1} at 373 K. For HIPS, the near room temperature values agree with those measured by Zhang, et al. [13] for PS (0.16 W m^{-1} K^{-1} at 305 to 510 K). However, these authors do not observe a substantial increase in the thermal conductivity with increasing temperature present in the current data. For HDPE, it is the midrange data, measured at 370 to 440 K, that demonstrate a reasonable agreement with the value of 0.22 W m^{-1} K^{-1} reported by Zhang, et al. (for polyethylene of unspecified density, in the same temperature range). For low temperatures (315 to 350 K), the thermal conductivity of HDPE measured here appears to be significantly lower than the value of 0.31 W m^{-1} K^{-1} observed by these authors (at 320 K). Discrepancies of similar magnitude between the data obtained by different laboratories were reported in earlier publications [13 and 14] (and were explained by the sensitivity of the thermal conductivity to subtle variations in the polymer structures).

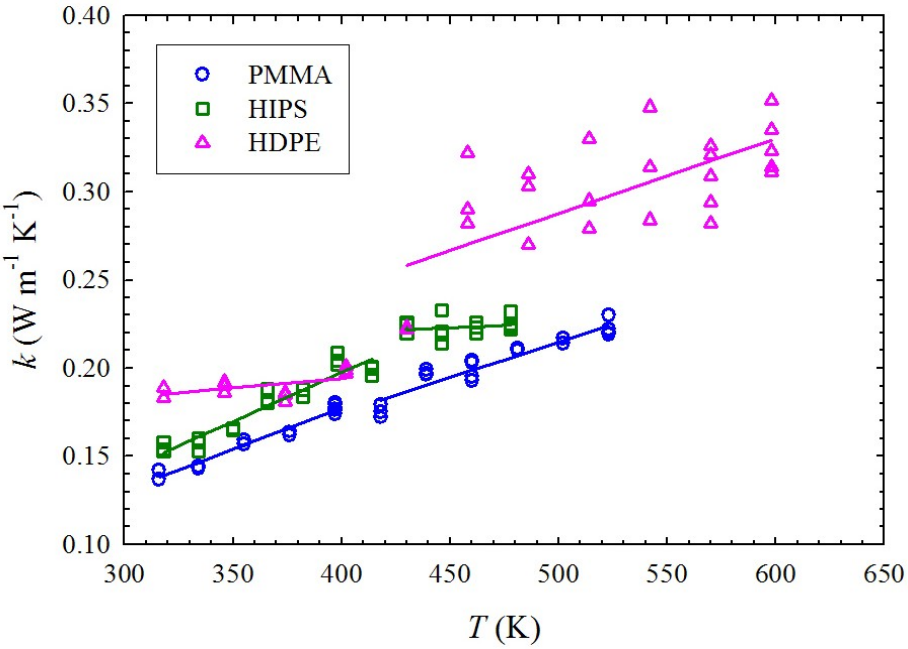

Figure 2. Thermal Conductivities

The thermal conductivity data obtained in this work were reduced by fitting them with a piecewise linear function of temperature:

$$k = \begin{cases} k_{S0} + k_{S1}T, & T < T_{trans} \\ k_{L0} + k_{L1}T, & T \geq T_{trans} \end{cases} \quad (7)$$

The fits are shown as lines in figure 2; the parameters are listed in table 5. T_{trans} values used in these fits are those obtained from the heat capacity measurements.

Table 5. Parameters (of equation 7) Describing Temperature Dependence of Thermal Conductivity

Polymer	k_{S0} (W m^{-1} K^{-1})	k_{S1} (W m^{-1} K^{-2})	T_{trans} (K)	k_{L0} (W m^{-1} K^{-1})	k_{L1} (W m^{-1} K^{-2})
PMMA	-0.01	4.7×10^{-4}	403	0.01	4.0×10^{-4}
HIPS	-0.02	5.5×10^{-4}	421	0.20	0.6×10^{-4}
HDPE	0.15	1.1×10^{-4}	407	0.08	4.2×10^{-4}

REFLECTIVITY AND ABSORPTION COEFFICIENT. The interaction of a polymeric material with a flux of infrared radiation can be described by two parameters, the reflectivity (r) and absorption coefficient (α). In general, these parameters strongly depend on the radiation wavelength and may also depend on the material's temperature. Capturing these dependencies leads to a complex radiative energy transfer model that requires a lot of experimental data, which are not readily available. The studies by Hallman, et al. [15] and Tsilingiris [16] represent rare attempts to provide a simplified quantitative description of this interaction. In the former study, wavelength-dependent reflectivities measured for several common plastics were averaged over emissive power distributions of a blackbody at several temperatures. The average reflectivity values corresponding to the materials used in the current study are listed in table 6. These values were obtained for a blackbody temperature of 1000 K, which is the closest match to radiant heater temperatures used in the burning rate measurements (described below).

Table 6. Parameters Describing Absorption of Radiative Heat

Polymer	r	α (m^{-1})
PMMA	0.15	2700
HIPS	0.14	2700[a]
HDPE	0.08	1300

[a] This value is a crude estimate.

Tsilingiris performed calculations of the total transmissivity (τ) of 5×10^{-5}- to 5×10^{-3}-m-thick polymer films to blackbody radiation. The author also provided an expression (based on the assumption of exponential attenuation) that relates the transmissivity and absorption coefficient:

$$\alpha = \frac{2\ln(1-r) - \ln\tau}{l} \tag{8}$$

where l is the polymer film thickness. This expression (together with the average reflectivities determined by Hallman, et al.) was used to calculate the absorption coefficients listed in table 6. The transmissivity data used in these calculations were obtained for a blackbody temperature of 873 K, which was the highest temperature used in the study by Tsilingiris. HIPS was not among the materials analyzed in that study. Here, it was assumed that the absorption coefficient for this polymer is equal to that of PMMA.

DECOMPOSITION KINETICS AND THERMODYNAMICS. The kinetics of polymer decomposition was studied using a Mettler Toledo TGA/SDTA851^e thermogravimetric analyzer. Polymer samples of 2×10^{-6} to 5×10^{-6} kg were heated from 373 to 1003 K at the rate of 0.05 K s^{-1}, 0.17 K s^{-1}, and 0.5 K s^{-1}. The experiments were conducted in a nitrogen atmosphere (the sample compartment was continuously purged with 6×10^{-7} m^3 s^{-1} of ultra-high purity nitrogen). The rate constants of decomposition (which was assumed to be a first order reaction) were calculated by numerical differentiation of mass loss data:

$$k_D = \frac{\Delta m}{(m_{res} - m)\Delta t} \tag{9}$$

where m is the current mass; Δm is the change in this mass during a short time Δt; and m_{res} is the residual mass at the end of experiment. The rate constants (calculated using Δt = 3 s) are plotted in Arrhenius coordinates in figure 3.

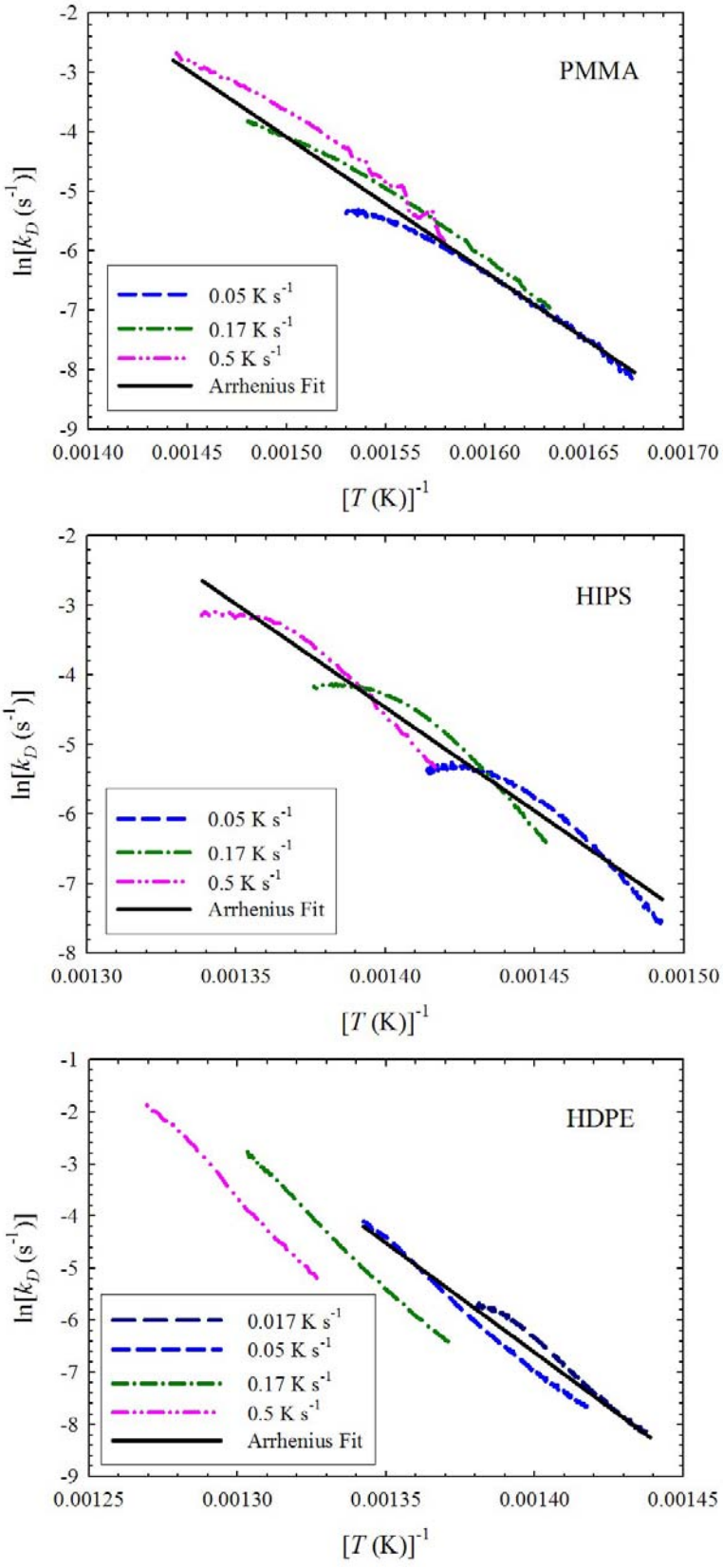

Figure 3. Rate Constants of Decomposition Reactions

For PMMA and HIPS, the rate constants can be fit reasonably well by the Arrhenius expression (equation 4). The pre-exponential factors and activation energies obtained for these polymers are listed in table 7. For HDPE, the rate constants show a systematic dependence on heating rate. One possible explanation of this dependence is that the mass loss is partially controlled by the rate of delivery of heat into the sample, which means that, during the decomposition, the sample does not keep up with the set heating rate. The results of an additional thermogravimetric experiment performed at 0.017 K s^{-1} support this explanation. These results show that when the heating is sufficiently slow (0.05 to 0.017 K s^{-1}), the heating rate dependence becomes insignificant (see figure 3). Therefore, the Arrhenius parameters for the decomposition of HDPE, which are listed in table 6, were determined by fitting only the low heating rate data (which, presumably, are not affected by heat transfer).

Table 7. Parameters Describing Decomposition Reactions

Polymer	A (s^{-1})	E (J mol^{-1})	h_D (J kg^{-1})	h_C (J kg^{-1})
PMMA	8.5×10^{12}	1.88×10^{5}	8.7×10^{5}	2.41×10^{7}
HIPS	1.2×10^{16}	2.47×10^{5}	1.0×10^{6}	3.81×10^{7}
HDPE	4.8×10^{22}	3.49×10^{5}	9.2×10^{5}	4.35×10^{7}

The heats of the decomposition reactions (h_D) were measured in a previous study [10]. They are listed in table 7. Also listed in table 7 are the heats of combustion of volatile decomposition products (h_C). Note that, unlike h_D, positive h_C represents an exotherm. Both h_D and h_C were normalized by the initial sample mass. The heats of combustion were determined using a microscale combustion calorimeter operating in the controlled thermal decomposition mode [17]. The pyrolysis was performed in a nitrogen atmosphere by heating a small (2×10^{-6} to 4×10^{-6} kg) sample of material from 373 to 1173 K at the rate of 1 K s^{-1}. Under these conditions, PMMA and HDPE volatilized completely, while HIPS produced 2% (of the initial sample mass) of nonvolatile residue. In the thermogravimetric experiments described above, all materials left behind small amounts, 1% to 4%, of residue.

UNCERTAINTIES IN PROPERTIES. The uncertainties in property values were determined from the scatter of the data and expressed as ±2 normalized standard errors (the standard errors were normalized by the corresponding values of the mean). The uncertainties in reported heat capacities, the heat of melting, heats of decomposition, and thermal conductivities were determined to be ±15%. The uncertainty in densities is ±5%. The uncertainties in the heats of combustion and activation energies are less than ±3%; the uncertainty in the Arrhenius pre-exponential factors is around ±50%. The uncertainties in reflectivities and absorption coefficients could not be determined because of the lack of the necessary information in the corresponding literature sources. Crude estimates of these uncertainties are ±20% and ±50%, respectively.

BURNING RATE MEASUREMENTS.

SAMPLE PREPARATION. Polymer samples were prepared by compression-molding of one or several 0.1 m × 0.1-m-square pieces that were cut from supplied 6×10^{-3}-m-thick sheets. The pieces were laid on top of each other inside a square (0.105 × 0.105 m) metal mold and subjected to 2×10^{3} to 5×10^{3} kg of load, which was applied from the top. To soften the polymers, the compression was performed at elevated temperatures. HIPS and HDPE were compression-molded at 423 K. A somewhat higher temperature of 453 K was used for PMMA. After the compression was complete, the samples were cooled to room temperature, removed from the mold, and cut to 0.101- × 0.101-m or 0.080- × 0.080-m squares. The former size was used for cone calorimetry, the latter for gasification experiments. The samples were made in three thicknesses: thick, medium, and thin. The thick samples were 0.024 to 0.029 m; the medium samples were 7.7×10^{-3} to 9.4×10^{-3} m; and the thin samples were 3.0×10^{-3} to 3.4×10^{-3} m. The thickness variation within a single sample was less than 10%. No further conditioning of the samples was carried out.

CONE CALORIMETRY. The heat released by burning polymers was measured using a cone calorimeter built by Fire Testing Technology Limited. The standard setup, calibration, and measurement procedures [5] were followed. Polymer samples were mounted horizontally, using a specimen holder with the edge frame. The bottom of the holder was lined with a 0.013- to 0.025-m-thick Kaowool blanket (see table 1 for its properties), which rested on top of the 0.025-m-thick Kaowool M board. The bottom and sides of each sample were wrapped with 2×10^{-5}-m-thick aluminum foil. The HRR calculation was based on the measurement of oxygen, carbon monoxide, and carbon dioxide concentrations in dried exhaust gas.

The only deviation from the standard was in the distance between the bottom surface of the cone heater and the initial position of the top surface (face) of a polymer sample. This distance was set at 0.038 m (instead of 0.025 m specified in the standard). This was done to accommodate charring polymers that expanded during the tests. The results obtained for the charring polymers will be the subject of a separate future technical note. As a consequence of the distance adjustment, the gap between the face of a sample and a spark plug, which was used to ignite the sample, increased to 0.020 m (0.013 m is specified in the standard).

During the heat release measurements, EHF (provided by the cone heater) was set at 25, 50, or 75 kW m^{-2}. These settings, which approximately correspond to the heater temperatures of 860, 1040, and 1170 K, were obtained using a flux meter positioned at a location equivalent to the initial position of the center of the sample face. To understand whether these flux values provide an accurate representation of the external heat fluxes experienced by the samples during the tests, the following experiments were carried out. First, the flux meter was shifted horizontally from the central position in four different directions, as shown in figure 4. While this revealed 1 to 2 kW m^{-2} deviations from the set heat flux of 50 kW m^{-2}, the mean value for the off-center measurements was found to be the same as the flux measured at the center. Next, the flux meter was lowered by 0.01 m and the measurement of the off-center fluxes was repeated. In that case, the mean of the fluxes was found to be 92% of the set flux. The presence of the edge frame did not have a significant effect on these measurements.

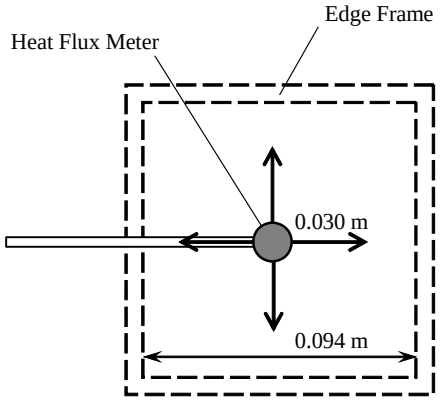

Figure 4. Heat Flux Measurements

Based on these observations, it was concluded that no correction was needed for EHF experienced by thin samples. Thick-sample EHF were corrected by a factor of 0.92 because, during the tests, the sample faces averaged about 0.01 m below their initial position. For medium samples, faces that averaged 4×10^{-3} m below their initial position used a proportionally smaller correction reflected in the correction factor of 0.97. All EHF values reported below (with the exception of those describing gasification experiments) have been corrected by the corresponding factors.

The heat release measurements performed at 49 kW m^{-2} of EHF on the samples of medium thickness were accompanied by temperature measurements. A hand-held probe was used to measure the temperature of the top layer of a burning sample (T_{top}). The measurement was performed by submerging the tip of the probe into the polymer melt, as shown in figure 5. An effort was made to hold the thermocouple bead (which was about 1×10^{-3} m in diameter) as close as possible (but still below) the top surface of the sample. During each measurement, the probe was kept submerged for 25 s. The temperature value was obtained by averaging the readings collected during the last 17 s. The temperature of the sample bottom surface (T_{bottom}) was also measured. A bead of type K thermocouple was attached to this surface (near its center) with a small piece of fiberglass tape. The temperature signal from this thermocouple was collected continuously throughout the heat release measurement.

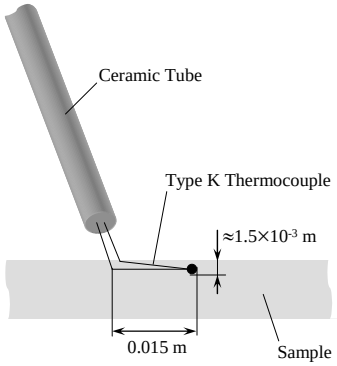

Figure 5. Measurement of the Top-Layer Temperature

GASIFICATION EXPERIMENTS. A gasification apparatus, somewhat similar to a cone calorimeter, was used to measure the rates of mass loss from polymer samples exposed to radiant heat. The apparatus, which was designed and constructed at the National Institute of Standards and Technology, consists of a load cell located in a sealed stainless-steel cylindrical chamber that is 1.70 m tall and 0.61 m in diameter. The heat flux is provided by a large (0.30 m in diameter) cone-shaped heater. The flux is controlled by adjusting the distance between the sample and the heater, which is held at a constant temperature of 1023 K. To maintain a negligible background heat flux, the interior walls of the chamber are painted black and water-cooled to 298 K. The tests were conducted in a nitrogen atmosphere, which removed any potential effects of the gas phase or surface oxidation on the gasification processes. A detailed description of the apparatus and testing procedures is given in reference 4.

Only the medium thickness samples of were used in the gasification experiments. The bottom and sides of each sample were wrapped with aluminum foil. The samples were positioned horizontally on the top of a 0.025-m-thick block of Foamglas insulation (see table 1 for its properties), which rested on the load cell. During the experiments, the faces of the samples were exposed to a constant EHF of 52 kW m^{-2}.

RESULTS

Every polymer studied in this work has exhibited some aspects of gasification behavior that may have affected the consistency of the experimental observations. A layer of foam that formed on the top of PMMA samples during gasification and combustion interfered with the top-layer temperature measurements. In some HIPS and HDPE cone calorimetry tests, a thin, black film formed on the top surface before ignition. The formation of the film, which occurred in less than 50% of the tests, was not repeatable and could not be associated with an exact set of conditions. In the case of HIPS, the film formation was also observed in the gasification apparatus. All experiments involving HDPE were accompanied by spattering and splashing of the polymer melt. This behavior resulted in a significant loss of sample in some cone calorimetry tests (further discussion of the impact of this behavior on the test results is given below). Despite the presence of the edge frame, thin samples of all polymers warped and formed bubbles early in the experiments. The samples usually regained their shapes around the time of ignition.

GASIFICATION.

The MLR versus time dependencies obtained from the gasification experiments are shown as open circles in figure 6 (this figure also contains the results of modeling, which are discussed below). The MLR of PMMA and HIPS have similar shapes. The MLR of HDPE behaved somewhat differently; it increased steeply toward the end of test. This increase may be caused partially by the inability of the aluminum foil wrap to contain the sample. The photographs of the sample taken in the beginning and end of this test show an expansion of the top-surface area by about 10%. This expansion is not taken into account in the calculation of MLR, which is normalized by the initial area of the sample face. No significant expansion of the top surface was observed in the PMMA or HIPS gasification experiments.

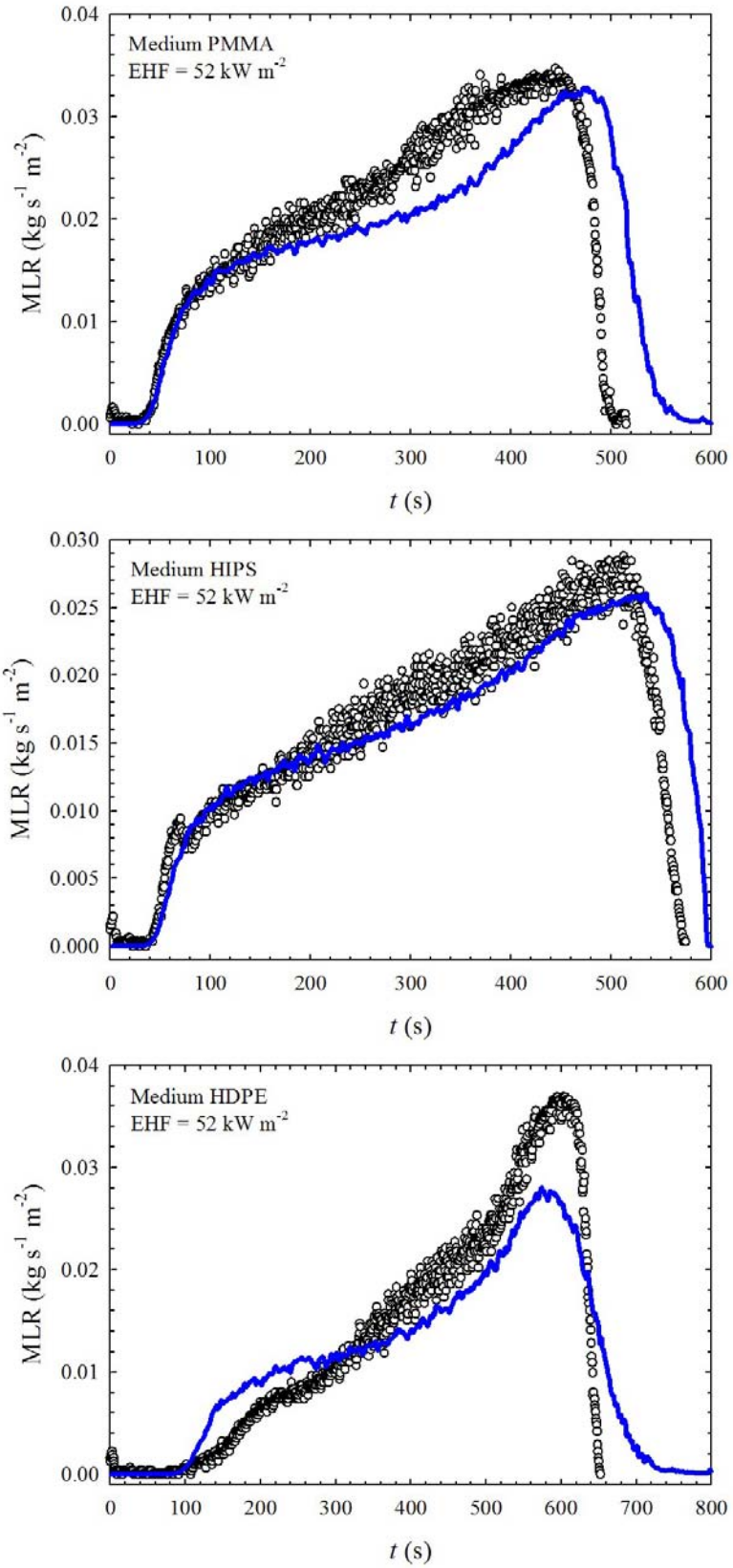

Figure 6. Results of Experimental (open circles) and Simulated (solid lines) Gasification Tests

CONE CALORIMETRY.

The HRR histories obtained from the cone calorimetry experiments are shown as open circles in figures 7, 8, and 9 (these figures also contain the results of modeling, which are discussed below). One significant difference between the shapes of the gasification MLR and cone HRR profiles obtained under similar conditions (medium thickness, EHF ≈ 50 kW m^{-2}) is the presence of an extended shoulder on the right-hand side of HRR maxima. This shoulder, which is most evident in the cone calorimetry data obtained for thin samples, was caused by a slow burning of the residual material located under the edge frame lip.

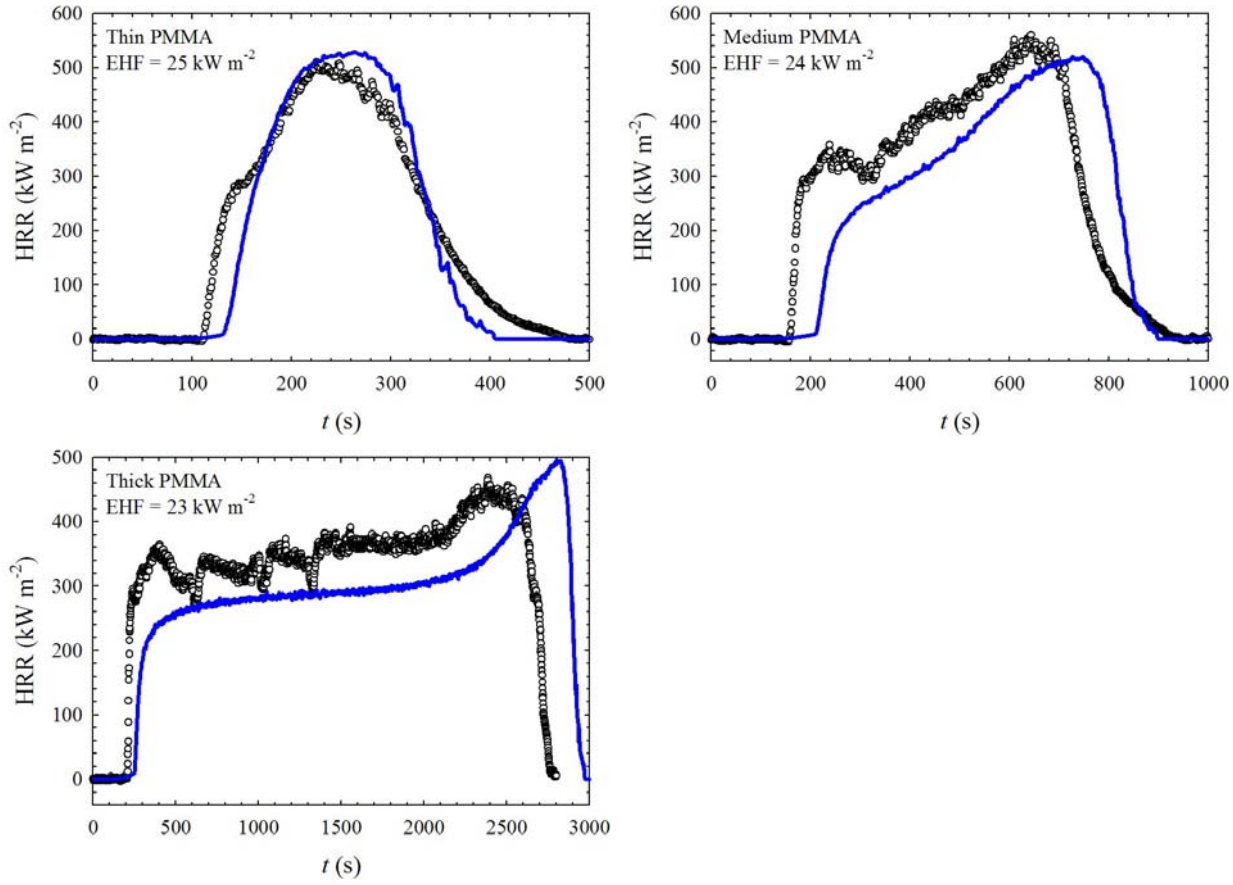

Figure 7. Results of Experimental (open circles) and Simulated (solid lines) PMMA Cone Calorimetry Tests

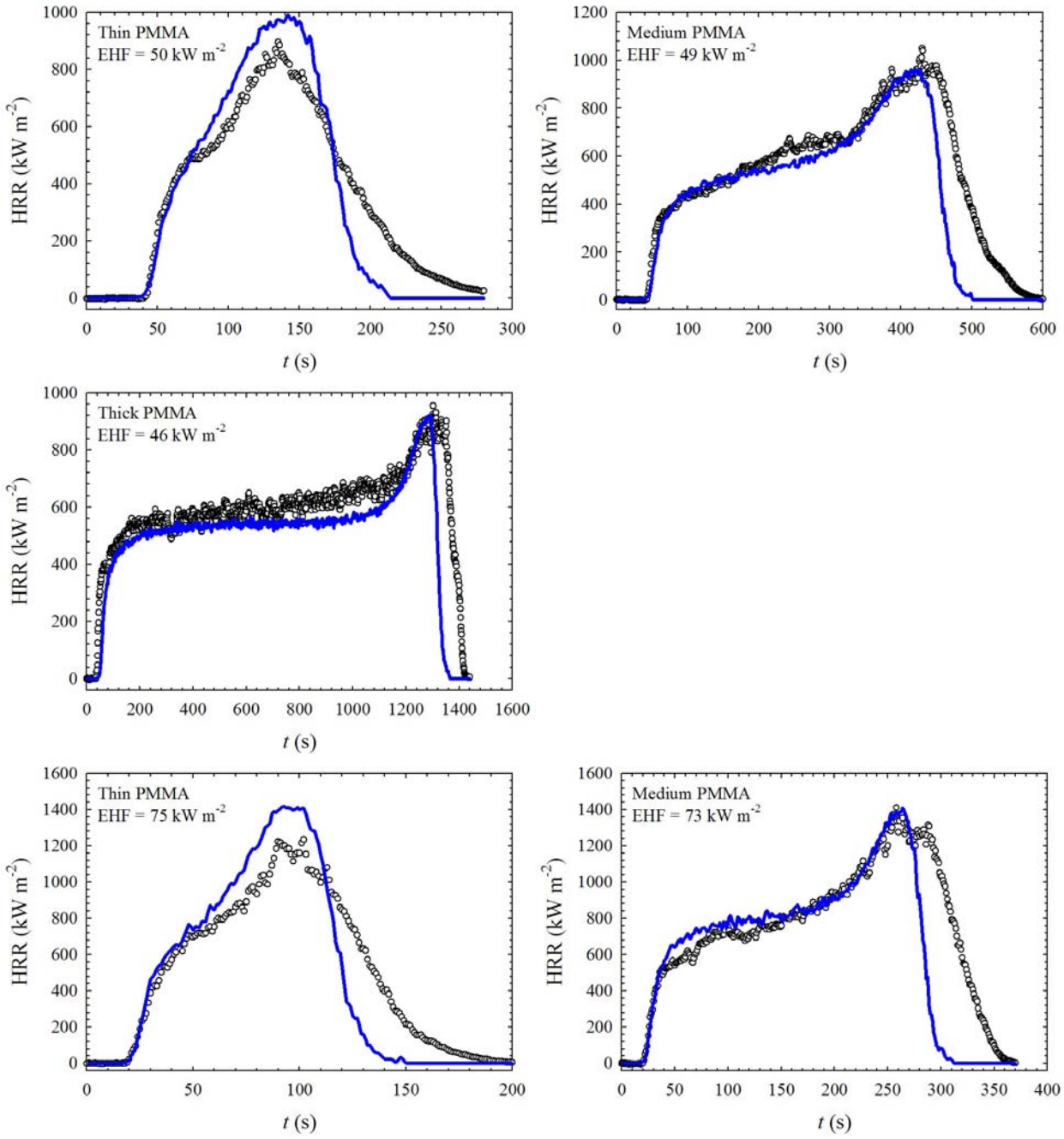

Figure 7. Results of Experimental (open circles) and Simulated (solid lines) PMMA Cone Calorimetry Tests (Continued)

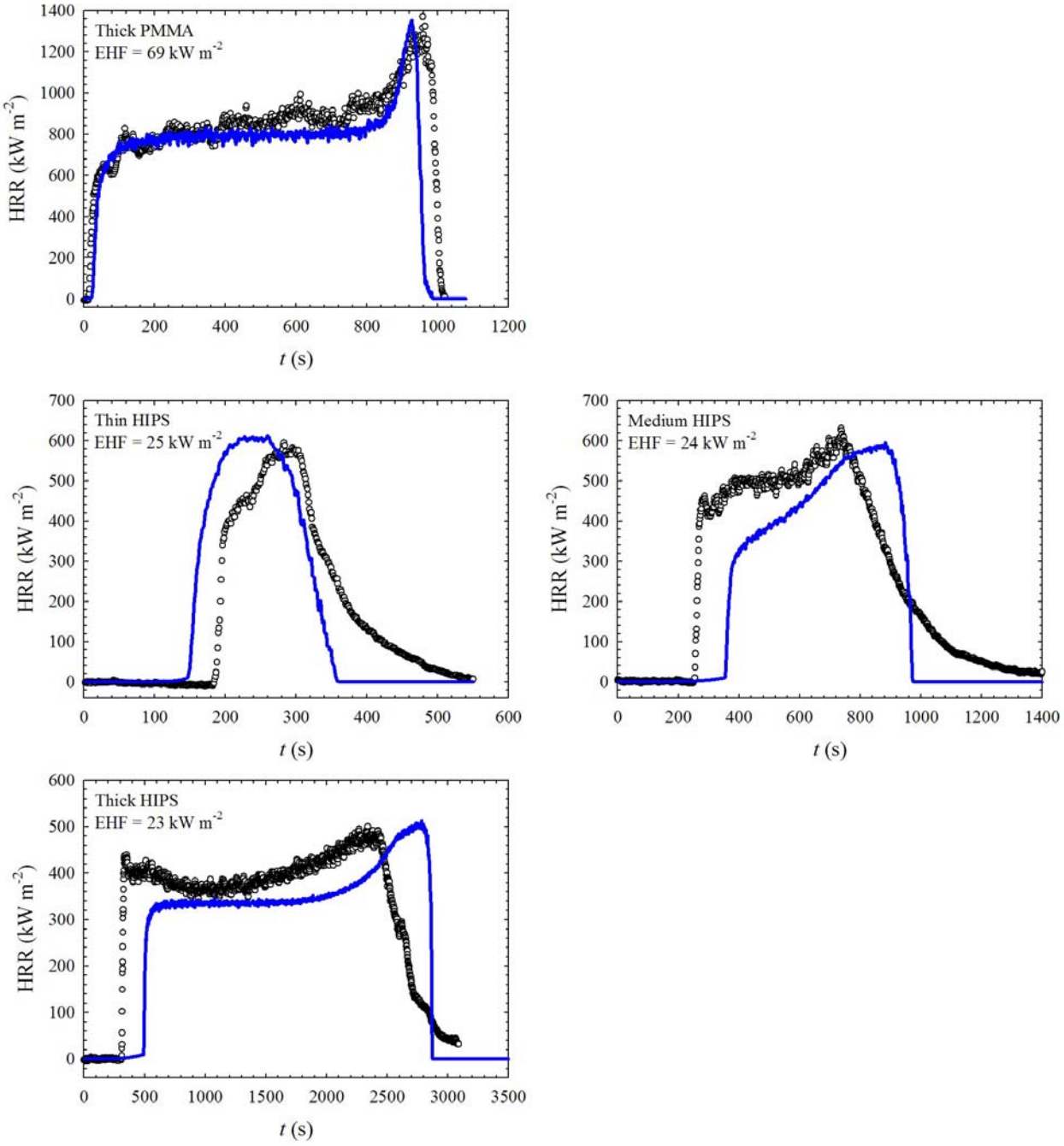

Figure 7. Results of Experimental (open circles) and Simulated (solid lines) PMMA Cone Calorimetry Tests (Continued)

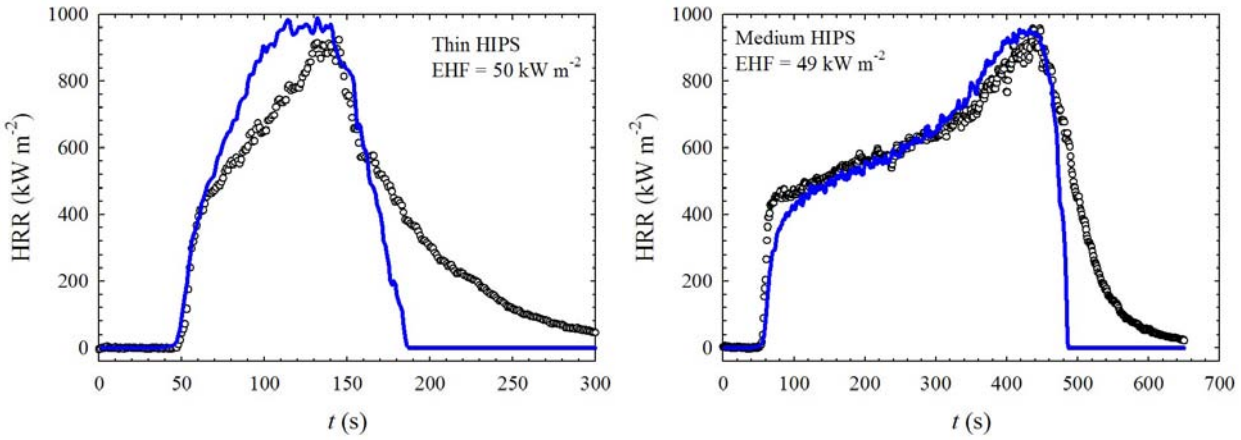

Figure 7. Results of Experimental (open circles) and Simulated (solid lines) PMMA Cone Calorimetry Tests (Continued)

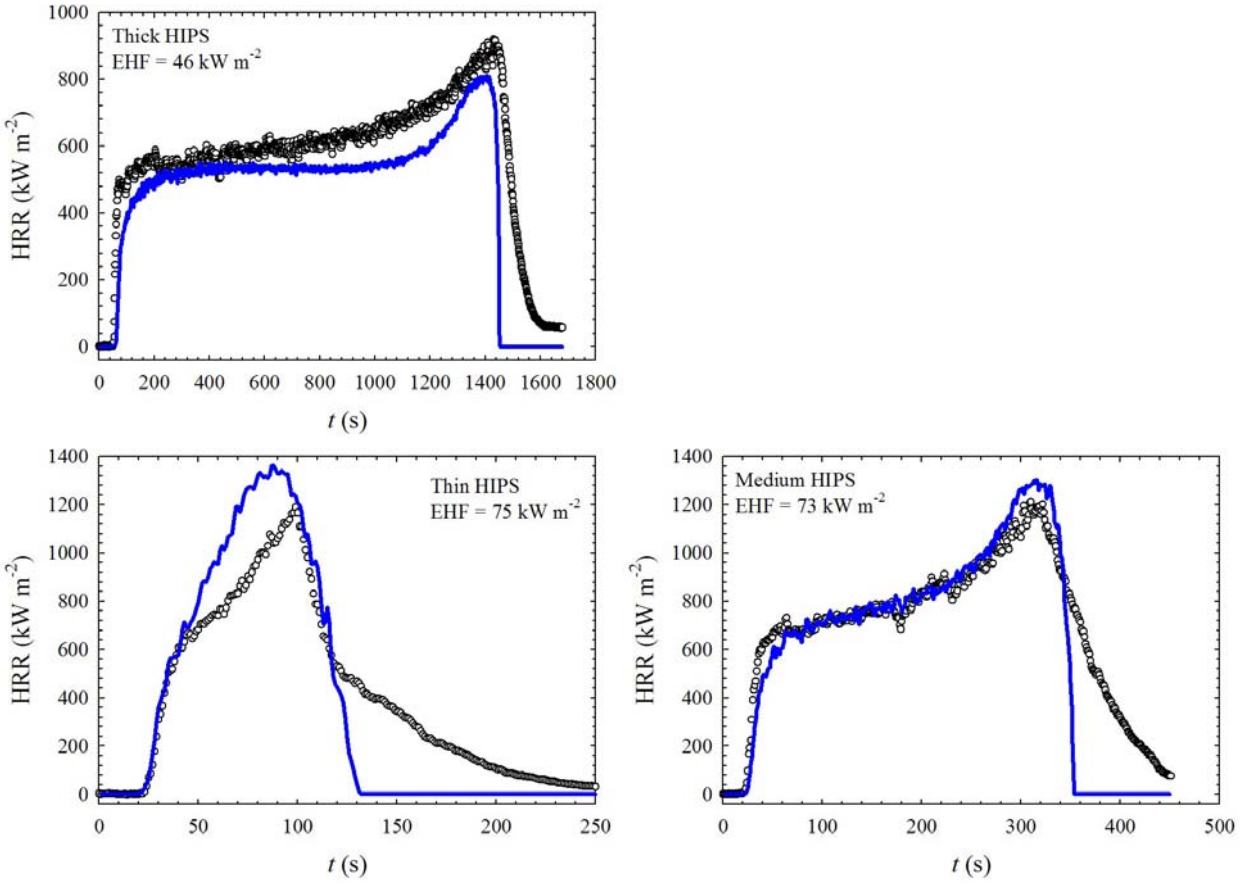

Figure 8. Results of Experimental (open circles) and Simulated (solid lines) HIPS Cone Calorimetry Tests

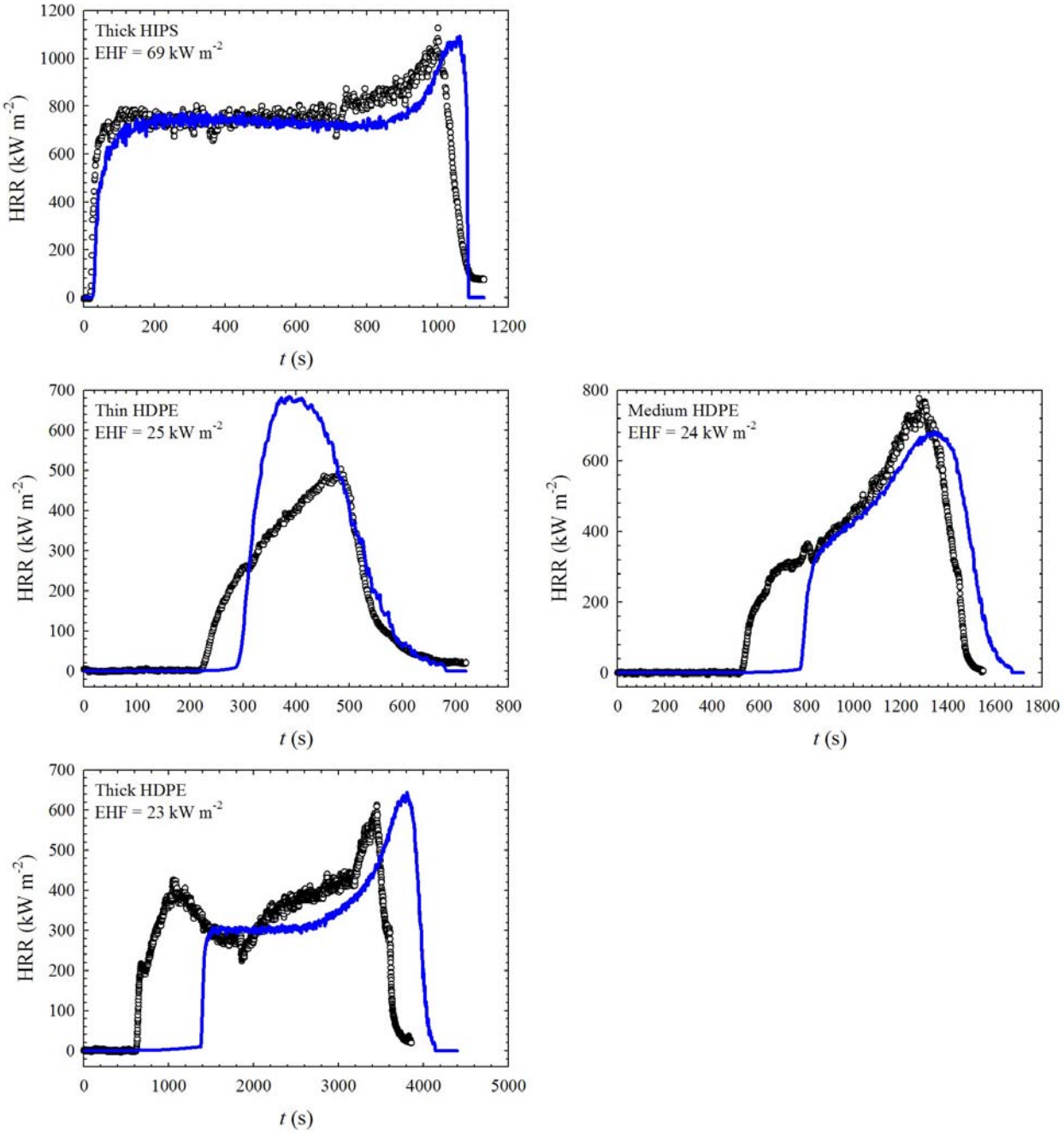

Figure 8. Results of Experimental (open circles) and Simulated (solid lines) HIPS Cone Calorimetry Tests (Continued)

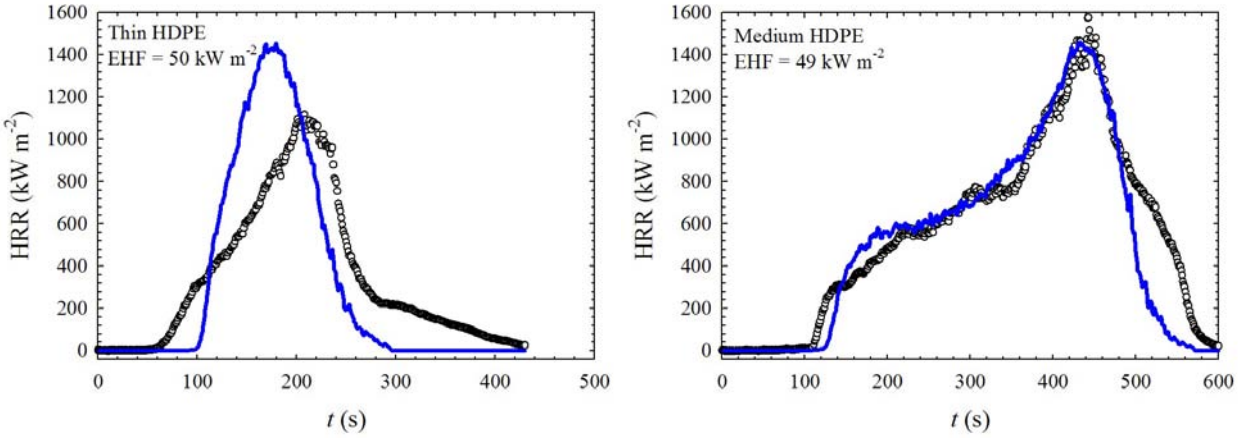

Figure 8. Results of Experimental (open circles) and Simulated (solid lines) HIPS Cone Calorimetry Tests (Continued)

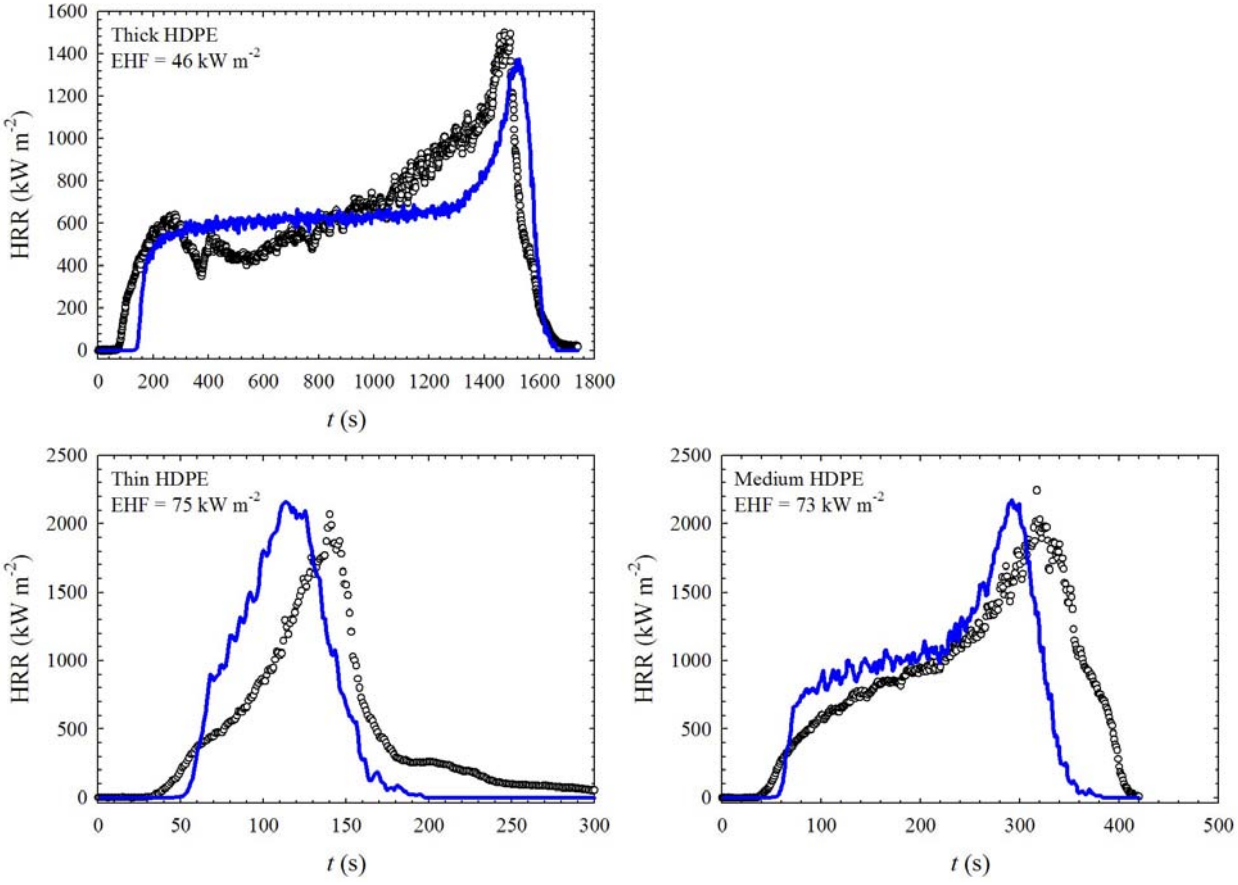

Figure 9. Results of Experimental (open circles) and Simulated (solid lines) HDPE Cone Calorimetry Tests

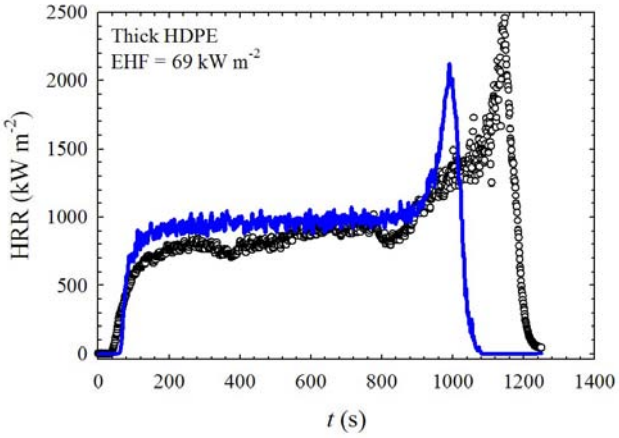

Figure 9. Results of Experimental (open circles) and Simulated (solid lines) HDPE Cone Calorimetry Tests (Continued)

Each HRR curve was recorded with a frequency of 1 s^{-1} and characterized by a set of four parameters: peak HRR, average HRR, time-to-ignition, and time-to-peak HRR. The peak HRR was calculated by determining the maximum value of 10 s moving average. The averaging was used to reduce the contribution of noise in the data to the value of the peak. The time-to-peak HRR was defined to be the time to the middle of the time interval corresponding to the peak HRR. The time-to-ignition was defined as the time when HRR exceeds the threshold of 10 kW m^{-2} for the first time (this value of the threshold gave the best agreement between the times-to-ignition determined from experimental HRR histories and the corresponding times of appearance of a sustained flame recorded by an operator).

The average HRR was obtained by integrating an HRR curve (numerically) from the time-to-ignition to the time of the end of test and subsequent division of the integral value by the length of the time period used in the integration. The time of the end of test was defined as the time of the final drop of HRR below 20 kW m^{-2}. The purpose of this threshold was to cutoff the part of the curve dominated by signal noise (which was notably higher in amplitude at the end of test than in the beginning). In most cone tests of HIPS performed at 46 to 75 kW m^{-2}, the value of HRR stayed above the threshold even after the complete cessation of flaming. In such cases, the time of the end of test was taken to be the time of flameout.

The parameter values characterizing the experimental HRR data are listed in table 8 (this table also contains the results of modeling, which are discussed below). As expected, both peak HRR and average HRR (obtained for the samples of the same material and thickness) increased with increasing EHF. The time-to-ignition and time-to-peak HRR also show a predictable trend, decreasing with increasing EHF. For PMMA and HIPS, the average HRR (obtained at about the same EHF) increased with increasing thickness; HDPE data do not show this trend. The peak HRR tends to be the highest for the medium-thickness samples. The time-to-peak HRR increased with increasing thickness. The time-to-ignition shows the same trend at low EHF (23-25 kW m^{-2}). On average, PMMA, HIPS, and HDPE release heat at comparable rates. However, HDPE did tend to produce higher peak HRR.

Table 8. Summary of the Results of Experimental/Simulated Cone Calorimetry Tests

Polymer	EHF ($kW\ m^{-2}$)	Sample Thickness*	Peak HRR ($kW\ m^{-2}$)	Average HRR ($kW\ m^{-2}$)	Time-to-Ignition (s)	Time-to-Peak HRR (s)
PMMA	25	thin	500 / 530	280 / 340	113 / 131	230 / 260
	24	medium	550 / 520	340 / 340	159 / 210	640 / 750
	23	thick	460 / 490	350 / 300	209 / 251	2380 / 2820
	50	thin	850 / 980	410 / 560	43 / 40	140 / 140
	49	medium	990 / 950	560 / 560	44 / 43	430 / 420
	46	thick	890 / 920	600 / 540	38 / 48	1310 / 1290
	75	thin	1180 / 1410	590 / 740	20 / 20	90 / 100
	73	medium	1350 / 1390	780 / 800	21 / 21	260 / 260
	69	thick	1270 / 1330	850 / 780	14 / 23	960 / 930
HIPS	25	thin	580 / 610	280 / 440	186 / 147	280 / 260
	24	medium	610 / 590	310 / 450	255 / 354	740 / 890
	23	thick	480 / 500	350 / 370	313 / 492	2420 / 2780
	50	thin	900 / 960	370 / 650	49 / 46	140 / 140
	49	medium	920 / 950	500 / 620	55 / 55	440 / 430
	46	thick	900 / 800	580 / 550	54 / 62	1440 / 1400
	75	thin	1140 / 1340	440 / 840	23 / 22	100 / 90
	73	medium	1180 / 1290	710 / 830	21 / 24	310 / 310
	69	thick	1050 / 1080	730 / 740	19 / 26	1000 / 1060
HDPE	25	thin	490 / 680	230 / 350	225 / 287	480 / 390
	24	medium	750 / 680	420 / 430	530 / 772	1310 / 1350
	23	thick	580 / 640	330 / 350	624 / 1377	3430 / 3810
	50	thin	1080 / 1430	390 / 710	60 / 100	200 / 170
	49	medium	1480 / 1440	660 / 700	99 / 124	450 / 430
	46	thick	1440 / 1360	610 / 640	74 / 140	1490 / 1520
	75	thin	1880 / 2120	520 / 940	33 / 51	140 / 120
	73	medium	2000 / 2140	940 / 990	38 / 56	320 / 290
	69	thick	2350 / 2040	910 / 970	39 / 61	1140 / 990

* Thin, medium, and thick are used to refer to 3.0×10^{-3} to 3.4×10^{-3} m, 7.7×10^{-3} to 9.4×10^{-3} m, and 0.024 to 0.029 m ranges of thickness, respectively.

To evaluate repeatability of the HRR measurements, the cone calorimetry experiments performed on medium samples at 49 $kW\ m^{-2}$ were repeated five times. The results are shown in figure 10. The repeatability of the HRR data obtained for PMMA and HIPS were reasonably

good, but were poor for HDPE. The poor repeatability is likely to be closely associated with a high mobility of the polymer melt. In each cone calorimetry experiment performed on HDPE (including those the results of which are shown in figure 9 and table 8), a fraction of the sample spilled onto the outer surface of the edge frame and burned. Another fraction escaped burning by splashing upon the cover of the load cell and leaking inside the edge frame. The unburned fraction (which was determined by collecting and weighing the material that survived the test) varied between 4% and 16% of the initial sample mass. The only exception was the cone calorimetry test of a thin HDPE at 25 kW m^{-2}. In this case, the unburned fraction reached 33%.

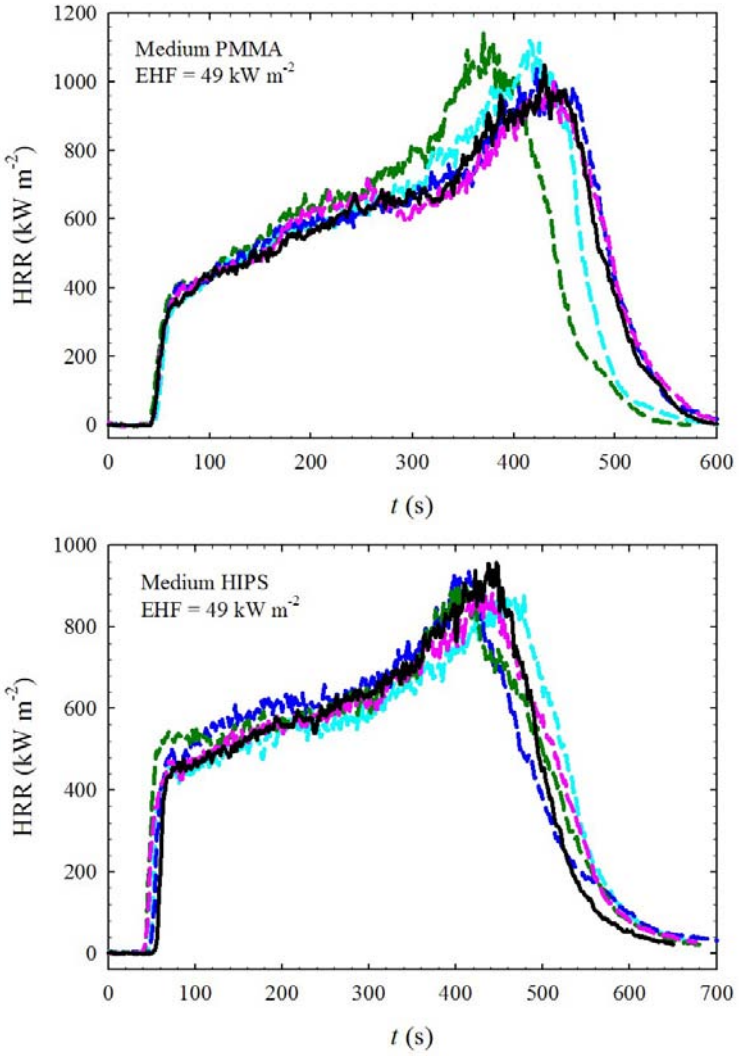

Figure 10. Repeatability of Cone Calorimetry Experiments (The HRR histories that have already been shown in figures 7, 8, and 9 and summarized in table 8 are depicted as solid lines.)

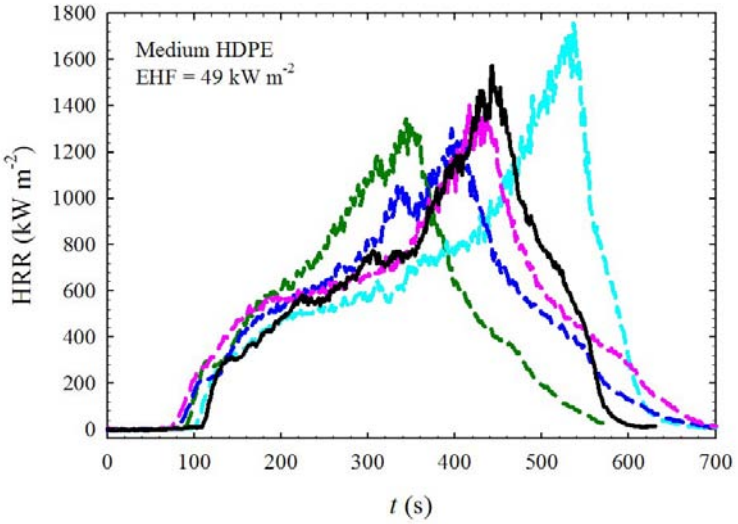

Figure 10. Repeatability of Cone Calorimetry Experiments (The HRR histories that have already been shown in figures 7, 8, and 9 and summarized in table 8 are depicted as solid lines.) (Continued)

The peak HRR, average HRR, time-to-ignition, and time-to-peak HRR calculated for the curves shown in figure 10 were used to provide an estimate of uncertainties in these parameters. The uncertainties, which were formulated to represent the minimum significant difference between the results of two tests, were calculated by taking two standard deviations of the difference in the value of a parameter and normalizing them by the mean of this parameter. The results of these calculations are given in table 9. As expected, the uncertainties reflect the HRR curve repeatability. For the experiments involving PMMA and HIPS, the uncertainties are comparable (with the exception of the uncertainty in the time-to-ignition). For HDPE, they are considerably higher.

Table 9. Uncertainties in Parameters Characterizing Experimental HRR Histories

Parameter / Polymer	Peak HRR (%)	Average HRR (%)	Time-to-Ignition (%)	Time-to-Peak HRR (%)
PMMA	17	7	12	17
HIPS	10	6	34	15
HDPE	36	28	35	45

The HRR data collected in the cone calorimetry experiments were also used to determine the total heat released. The total heat was calculated by taking the value of the integral used in the calculation of average HRR and normalizing it by the initial sample mass. In the case of HDPE, the sample mass was corrected by the amount of unburned sample. The total heat obtained from

the experiments performed on the same material shows little scatter and has no apparent dependence on EHF or sample thickness. The mean values of the total heat released by PMMA, HIPS, and HDPE are 2.41×10^7 J kg^{-1}, 2.90×10^7 J kg^{-1}, and 4.24×10^7 J kg^{-1}, respectively. The mean value uncertainties (which were calculated as ±2 normalized standard errors) are smaller than ±3%. The ratio of the total heat and h_C (listed in table 7) provides a measure of efficiency of the cone calorimetry gas-phase combustion process. For PMMA and HDPE, this efficiency is close to 100%. For HIPS, it is about 75%.

The amount of residue that PMMA and HDPE left inside aluminum foil wrap after the completion of a cone calorimetry test was always negligible. On the other hand, HIPS produced about 2% (of the initial sample mass) of white, flaky residue. This observation is consistent with the results of the microscale combustion calorimetry (discussed above). A slow smoldering of this residue is likely to be the reason why the HRR had a tendency to stay above 20 kW m^{-2} even after the complete cessation of flaming.

The results of the top layer and bottom-surface temperature measurements are shown as open circles in figure 11 and dashed lines in figure 12. These figures also contain the results of modeling, which are discussed below. These measurements were conducted during the same cone calorimetry experiments that were used to assess the repeatability of HRR histories. Most T_{top} values were obtained by probing the area near the center of the sample face. Probing a peripheral area (near the edge of the edge frame) did not produce significantly different results. All T_{top} measurements were performed after ignition. The data suggest that the top surface of HIPS is hotter than that of PMMA, while the surface of HDPE is the hottest. There is a significant scatter (about ±30 K) in the T_{top} data. A possible dependence of T_{top} on time is obscured by this scatter.

Unlike T_{top}, T_{bottom} show a clear trend, increasing with time. The repeatability of T_{bottom} is good in the beginning of the experiments; however, it deteriorates toward the end. This deterioration, which happens particularly early in the experiments involving HDPE, is most likely caused by a strain in the thermocouple wires pressed against the bottom surface. When the thickness and/or viscosity of the sample became sufficiently low, this strain made the thermocouple bead move upward (through the sample). Therefore, the lowest values of T_{bottom}, which presumably correspond to the bead position closest to the bottom surface, are likely to be the most accurate.

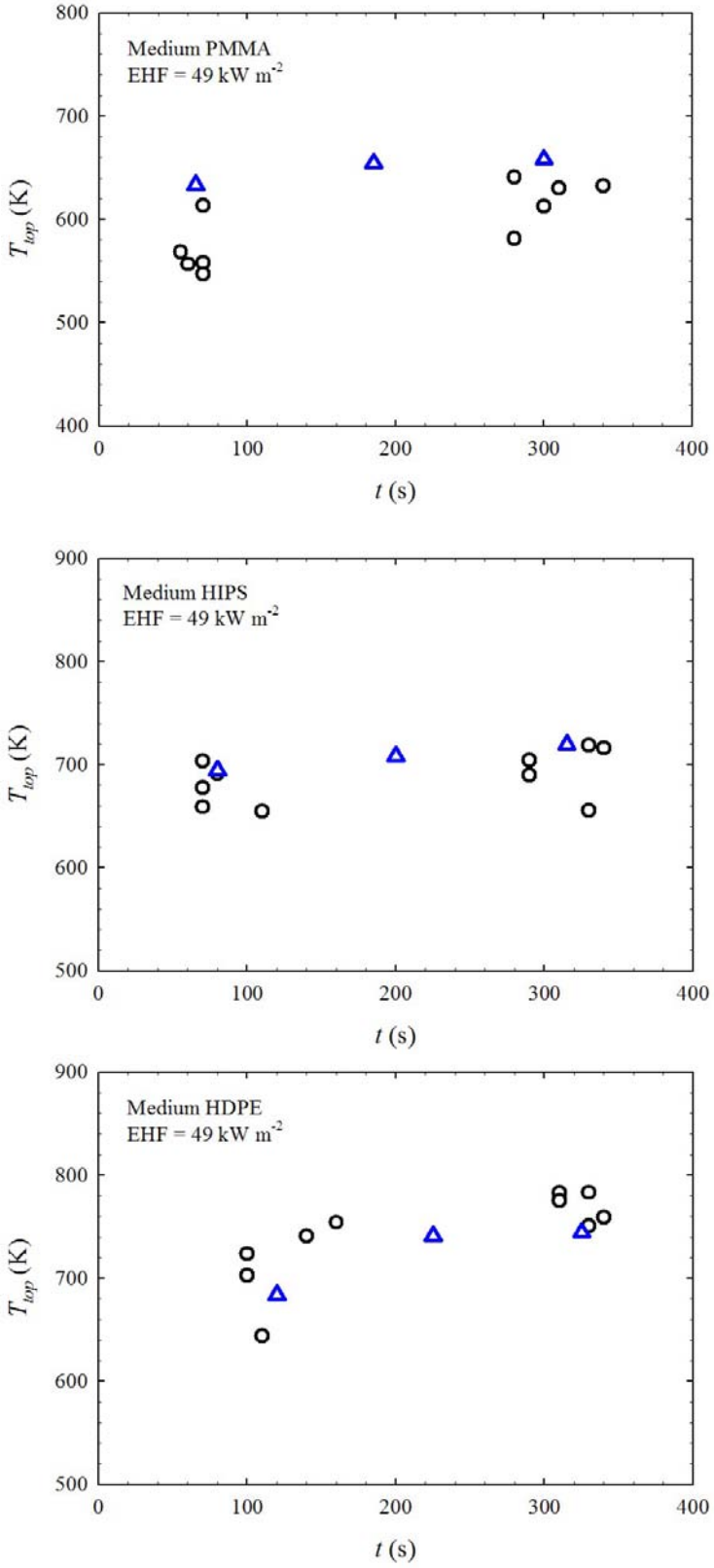

Figure 11. Top-Layer Temperatures Obtained From Experiments (open circles) and Simulations (open triangles)

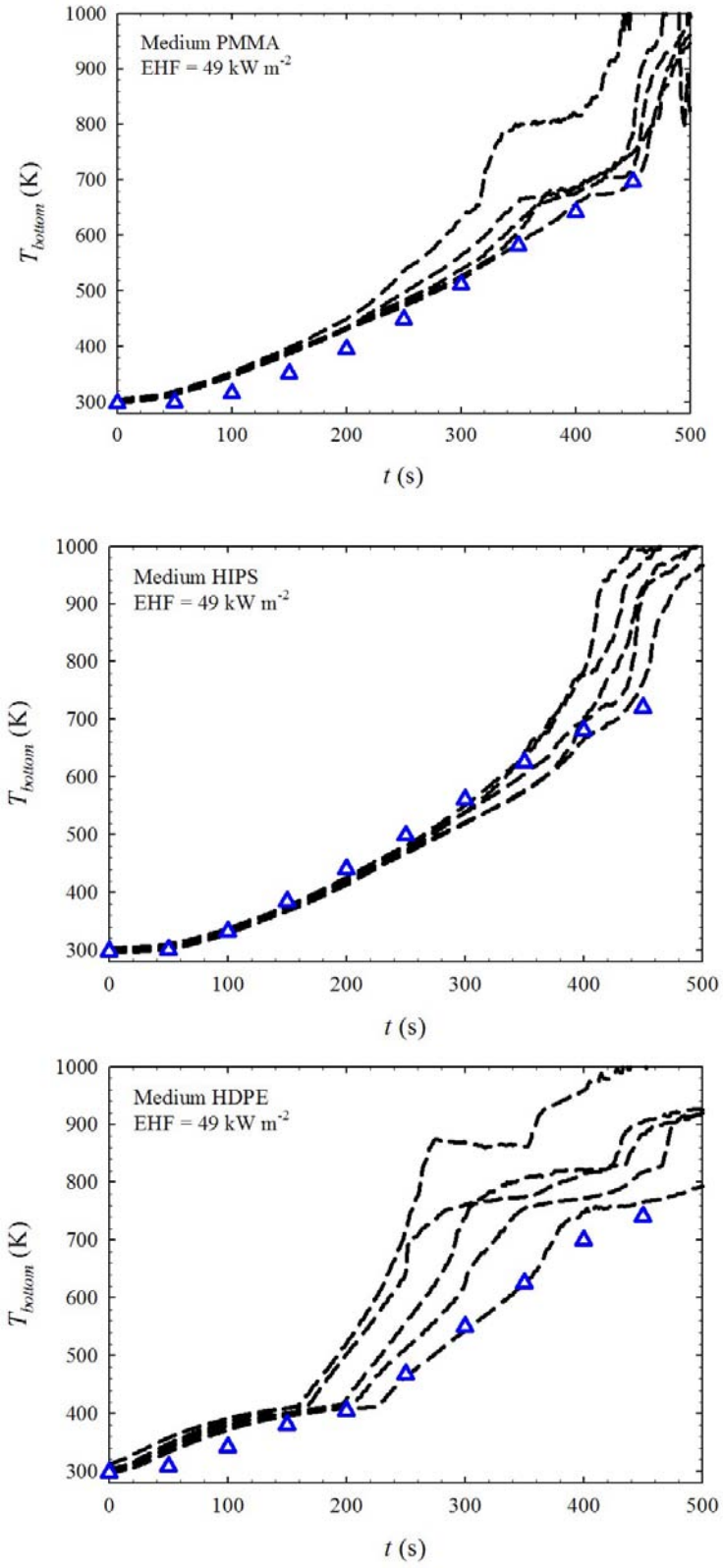

Figure 12. Bottom-Surface Temperatures Obtained From Experiments (dashed lines) and Simulations (open triangles)

UNCERTAINTIES IN MODELING OF EXPERIMENTS.

The results of modeling of the gasification tests are shown as solid lines in figure 6. Taking into account significant uncertainties in the material properties and the fact that no adjustable parameters were used in the simulations, the agreement between the model of PMMA and HIPS and the corresponding experiments is excellent. In the case of HDPE, the maximum MLR predicted by the model is about 25% lower than that observed in the experiment. From this point on, every relative difference is normalized by the mean of the values that are being compared. However, about half of this difference can be attributed to the sample surface expansion, which occurred during the experiment on HDPE.

Modeling of the cone calorimetry tests requires the knowledge of heat flux from the flame. The value of this flux was determined by fitting the experimental HRR history obtained for a medium sample exposed to 49 kW m^{-2} of EHF. The flame heat flux specified in the model was adjusted in 1 kW m^{-2} increments until the best agreement between the simulated and experimental HRR curve was identified. The quality of the agreement was determined on the basis of a visual inspection. For PMMA, HIPS, and HDPE, the value of the flame heat flux was found to be 12 kW m^{-2}, 11 kW m^{-2}, and 11 kW m^{-2}, respectively. For PMMA and HDPE, an assumption that this flux does not depend on EHF or sample thickness resulted in a reasonable overall agreement between the model and experiments. The results of the modeling are shown as solid lines in figures 7 and 9. For HIPS, this assumption did not produce satisfactory results. While a good agreement was achieved at intermediate EHF (46 to 50 kW m^{-2}), the model grossly underpredicted the experimental HRR at low EHF and overpredicted the data at high EHF.

Several potential sources of these discrepancies were analyzed including the effects of uncertainties in material properties. The most significant improvement in the agreement with the experiment was achieved by assuming that the flame produced by HIPS attenuates the radiation from the cone heater. A combination of a 25% reduction in EHF and 24 kW m^{-2} flame heat flux (both of which were assumed to be independent of EHF and sample thickness) resulted in the simulated HRR histories that are shown as solid lines in figure 8. This assumption is consistent with an observation of a large amount of soot produced in the HIPS cone calorimetry tests. While no quantitative measurements were carried out, the amount of soot that was found on the gas-sampling filter after a HIPS experiment was always many times larger than that deposited by a similar-sized PMMA or HDPE sample. The soot particles forming in the flame are expected to block some external radiation directed toward the sample and, at the same time, boost radiative energy transfer from the flame.

The simulated HRRs were characterized by calculating the peak HRR, average HRR, time-to-ignition, and time-to-peak HRR (these parameters were computed using the exact same methodology that was applied to the experimental HRR curves). The results of the calculations are given in table 8. The peak HRR and time-to-peak HRR agree well with the corresponding experimental values for all polymers and under all conditions. In over 90% of cases, the relative difference is within the experimental uncertainties (listed in table 9). The largest differences between the simulated and experimental parameters (32% for peak HRR and 21% for time-to-peak HRR) correspond to the test performed on a thin HDPE at 25 kW m^{-2} of EHF. This is the

experiment during which an extraordinarily high fraction of the sample (33%) escaped the sample container.

Many average HRRs obtained from the simulations are notably higher than the corresponding experimental values. The largest differences are observed for thin samples. For thin HIPS at 75 kW m^{-2}, the relative difference reaches the highest value of 63%. These differences are a consequence of the presence of an extended right-hand-side shoulder in the experimental HRR histories. As explained previously, this shoulder is a result of a slow-burning residual material located under the lip of the edge frame. This process is not captured by the one-dimensional model.

For PMMA and HIPS, the model predicts experimental times to ignition reasonably well. The relative difference is within the experimental uncertainty for about 70% of all tests performed on these materials. However, in the case of HDPE, most of the times to ignition are considerably overestimated by the model. A high sensitivity of this parameter to EHF is probably the key reason for the discrepancies (including those observed for PMMA and HIPS). The largest relative difference of 75% between the simulated and experimental time-to-ignition is observed for the test conducted on a thick HDPE at 23 kW m^{-2}. These times can be brought into a complete agreement (the difference of less than 6%) by increasing the model EHF by 4 kW m^{-2}. There are two factors that may justify this increase. The heat flux measurements (described above) indicate that, in the cone calorimeter, EHF decreases with decreasing sample thickness. A simplifying assumption that was used in this study is that EHF can be represented by a constant value, which corresponds to half the initial thickness. Eliminating this assumption would lead to 2 kW m^{-2} increase in the pre-ignition EHF. These measurements also show that EHF is not completely uniform. The fluctuations of the heat flux over the sample surface can account for the other 2 kW m^{-2}. The effects of nonuniformity of EHF on the ignition process were evident in many low EHF cone calorimetry experiments. In these experiments, only a fraction of the top sample surface was initially ignited. It usually took several seconds for the flame to spread to the whole surface.

The values of T_{top} and T_{bottom} obtained from the simulations are shown as open triangles in figures 11 and 12. T_{top} was determined by calculating the mean of the temperatures of the elements comprising the top 1.5×10^{-3} m thick layer of the object (this thickness corresponds to the depth that was probed experimentally). The temperature of the bottom element of the polymer layer was assumed to correspond to T_{bottom}. For HIPS and HDPE, the values of T_{top} are in good agreement with the experiment. For PMMA, the simulated T_{top} values are slightly higher than those determined experimentally, which may be a consequence of a systematic error in the positioning of the temperature probe due to the presence of foam on the sample surface. Taking into account that the lowest measured bottom surface temperatures are probably the most accurate, T_{bottom} are predicted reasonably well for all polymers.

DISCUSSION

The results of this study demonstrate that a one-dimensional numerical pyrolysis model can be used to predict the outcome of gasification and cone calorimetry experiments performed on noncharring polymers. The predictions require the knowledge of chemical (decomposition

kinetics and thermodynamics), thermal (density, heat capacity, and thermal conductivity), and optical (reflectivity and absorption coefficient) properties of the material. Most of these properties can be measured in milligram-scale laboratory tests or calculated from molecular structure using group additivity [18].

To predict the results of a cone calorimetry experiment, the knowledge of the heat flux from the flame onto the material surface and the total heat released in the flame are also required. In this study, the flame heat flux was determined by fitting an experimental heat release rate curve with the model. The total heat released was also calculated from this curve. It was shown that these parameters do not depend on the external heat flux (from the cone heater) or initial sample thickness, which means that the model can be used to extrapolate the results of a cone calorimetry experiment to a different set of conditions (i.e., different external heat flux, initial sample thickness, or backing material). In the case of a highly sooting polymer (such as high-impact polystyrene), two experimental heat release rate curves (obtained at different external heat fluxes) are required to perform the extrapolation because both the flame heat flux and the fraction of the external radiation absorbed by the flame need to be determined.

Recently, Beaulieu and Dembsey [19] have carried out direct measurements of the flame heat flux using the advanced flammability measurements apparatus (the setup that is similar to a cone calorimeter). The results of their measurements, 20 kW m^{-2} for black poly(methylmethacrylate) and 11 kW m^{-2} for black poly(oxymethylene), fall within the range obtained in this work (11 to 24 kW m^{-2}). This relatively narrow range suggests that the flame heat flux is not very sensitive to the chemical structure of the polymer. Thus, for a cone calorimetry test of a horizontally oriented polymeric sample, 16 kW m^{-2} (the mean of the values obtained in this study and reported by Beaulieu and Dembsey) should serve as a good first-order approximation of the incident flame heat flux. The total heat released can also be estimated without performing a cone calorimetry test. This heat can be approximated by the heat of combustion of volatile decomposition products, which can be easily measured using microscale combustion calorimetry [17] or calculated from atomic composition [20].

It should be noted that, regardless of the accuracy of the input parameters, the predictive ability of the model is bound by certain fundamental limitations. These limitations arise from a high sensitivity (or highly nonlinear response) of some aspects of the material behavior to experimental conditions. In particular, the accuracy of prediction of the time-to-ignition is expected to decrease rapidly as the external heat flux approaches its critical value (the minimum value required for sample ignition). Near the critical heat flux, a small (1% to 5%) uncertainty in this flux may result in a very large (100% or more) variation in the time-to-ignition. The relatively poor agreement between the simulated and experimental times to ignition observed in this study at low external heat fluxes is believed to be a manifestation of this limitation.

REFERENCES

1. Vovelle, C., Delfau, J.L., Reuillon, M., Bransier, J., and Laraqui, N., "Experimental and Numerical Study of the Thermal Degradation of PMMA," *Combustion Science and Technology,* Vol. 53, 1987, pp. 187-201.

2. Staggs, J.E.J., "A Theory for Quasi-Steady Single-Step Thermal Degradation of Polymers," *Fire and Materials,* Vol. 22, 1998, pp. 109-118.

3. Di Blasi, C., "Analysis of Convection and Secondary Reaction Effects Within Porous Solid Fuels Undergoing Pyrolysis," *Combustion Science and Technology,* Vol. 90, 1993, pp. 315-340.

4. Austin, P.J., Buch, R.R., and Kashiwagi, T., "Gasification of Silicone Fluids Under External Thermal Radiation Part I. Gasification Rate and Global Heat of Gasification," *Fire and Materials,* Vol. 22, 1998, pp. 221-237.

5. ASTM Standard E 1354-04a, "Standard Test Method for Heat and Visible Smoke Release Rates for Materials and Products Using an Oxygen Consumption Calorimeter," ASTM International, West Conshohocken, Pennsylvania, 2007.

6. Stoliarov, S.I. and Lyon, R.E., "Thermo-Kinetic Model of Burning," FAA report DOT/FAA/AR-TN08/17, May 2008.

7. Stoliarov, S.I., and Lyon, R.E., "Thermo-Kinetic Model of Burning for Pyrolyzing Materials," *Proceedings of the Ninth International Symposium on Fire Safety Science*, 2008.

8. Holman, J.P., *Heat Transfer, Ninth Edition,* McGraw-Hill, Boston, Massachusetts, 2002.

9. Mark, J.E., ed., *Physical Properties of Polymers Handbook*, American Institute of Physics: Woodbury, New York, 1996.

10. Stoliarov, S.I. and Walters, R.N., "Determination of the Heats of Gasification of Polymers using Differential Scanning Calorimetry," *Polymer Degradation and Stability,* Vol. 93, 2008, pp. 422-427.

11. Lobo, H. and Cohen, C., "Measurement of Thermal Conductivity of Polymer Melts by the Line-Source Method," *Polymer Engineering and Science,* Vol. 30, 1990, pp. 65-70.

12. Brandrup, J., Immergut, E.H., Grulke, E.A., Abe, A., and Bloch, D.R., eds., *Polymer Handbook, Fourth Edition,* John Wiley & Sons, New York, New York, 1999.

13. Zhang, X., Hendro, W., Fujii, M., Tomimura, T., and Imaishi, N., "Measurements of the Thermal Conductivity and Thermal Diffusivity of Polymer Melts With the Short-Hot-Wire Method," *International Journal of Thermophysics,* Vol. 23, 2002, pp. 1077-1090.

14. Fuller, T.R. and Fricke, A.L., "Thermal Conductivity of Polymer Melts," *Journal of Applied Polymer Science,* Vol. 15, 1971, pp. 1729-1736.

15. Hallman, J.R., Welker, J.R., and Sliepcevich, C.M., "Polymer Surface Reflectance-Absorptance Characteristics," *Polymer Engineering and Science*, Vol. 14, 1974, pp. 717-723.

16. Tsilingiris, P.T., "Comparative Evaluation of the Infrared Transmission of Polymer Films," *Energy Conversion and Management*, Vol. 44, 2003, pp. 2839-2856.

17. ASTM Standard D 7309 – 07, "Test Method for Determining Flammability Characteristics of Plastics and Other Solid Materials Using Microscale Combustion Calorimetry," ASTM International, West Conshohocken, Pennsylvania, 2007.

18. Van Krevelen, D.W., *Properties of Polymers, Third Edition*, Elsevier, Amsterdam, 1990.

19. Beaulieu, P.A. and Dembsey, N.A., "Effect of Oxygen on Flame Heat Flux in Horizontal and Vertical Orientations," *Fire Safety Journal*, Vol. 43, 2008, pp. 410-428.

20. Stoliarov, S.I., Williams, Q., Walters, R.N., Crowley, S., and Lyon, R.E., "Heats of Combustion of Brominated Epoxies," *Proceedings of the 2006 Symposium of the Society for the Advancement of Material and Process Engineering.*